This is a preprint, the final version is subject to change, of the American Mineralogist (MSA)
Cite as Authors (Year) Title. American Mineralogist, in press.
DOI: https://doi.org/10.2138/am-2018-6346

Revision 1

Gypsum, bassanite, and anhydrite at Gale crater, Mars

David T. Vaniman[1], Germán M. Martínez[2], Elizabeth B. Rampe[3], Thomas F. Bristow[4], David F. Blake[4], Albert S. Yen[5], Douglas W. Ming[3], William Rapin[6], Pierre-Yves Meslin[7], John Michael Morookian[5], Robert T. Downs[8], Steve J. Chipera[9], Richard V. Morris[3], Shaunna M. Morrison[10], Allan H. Treiman[11], Cherie N. Achilles[8], Kevin Robertson[12], John P. Grotzinger[6], Robert M. Hazen[10], Roger C. Wiens[13], Dawn Y. Sumner[14]

[1]Planetary Science Institute, Tucson, Arizona 85719, USA
[2]University of Michigan, Ann Arbor, Michigan 48109, USA
[3]NASA Johnson Space Center, Houston, Texas 77058, USA
[4]NASA Ames Research Center, Moffett Field, California 94035, USA
[5]Jet Propulsion Laboratory, California Institute of Technology, Pasadena, California 91109, USA
[6]Division of Geologic and Planetary Sciences, California Institute of Technology, Pasadena, California 91125, USA
[7]Institut de Recherche en Astrophysique et Planétologie, CNRS, UMR 5277, Toulouse, France
[8]Department of Geosciences, University of Arizona, Tucson, Arizona 85721, USA
[9]Chesapeake Energy, Oklahoma City, Oklahoma 73154, USA
[10]Geophysical Laboratory, Carnegie Institution for Science, Washington, DC 20015, USA
[11]Lunar and Planetary Institute – Universities Space Research Association, Houston, Texas 77058, USA
[12]Department of Earth, Environmental and Planetary Sciences, Brown University, Providence, Rhode Island 02912
[13]Los Alamos National Laboratory, Los Alamos, New Mexico 87545, USA
[14]Department of Earth and Planetary Sciences, University of California, Davis, California 95616, USA

ABSTRACT

Analyses by the CheMin X-ray diffraction instrument on Mars Science Laboratory show that gypsum, bassanite, and anhydrite are common minerals at Gale crater. Warm conditions (~6 to 30 °C) within CheMin drive gypsum dehydration to bassanite; measured surface temperatures and modeled temperature depth profiles indicate that near-equatorial warm-season surface heating can also cause gypsum dehydration to bassanite. By accounting for instrumental dehydration effects we are able to quantify the *in situ* abundances of Ca-sulfate phases in sedimentary rocks and in eolian sands at Gale crater. All three Ca-sulfate minerals occur together in some sedimentary rocks and their abundances and associations vary stratigraphically. Several Ca-sulfate diagenetic events are indicated. Salinity-driven anhydrite precipitation at temperatures below ~50 °C may be supported by co-occurrence of more soluble salts. An alternative pathway to anhydrite via dehydration might be possible, but if so would likely be limited to warmer near-equatorial dark eolian sands that presently contain only anhydrite. The polyphase Ca-sulfate associations at Gale crater reflect limited opportunities for equilibration, and presage mixed salt associations anticipated in higher strata that are more sulfate-rich and may mark local or global

environmental change. Mineral transformations within CheMin also provide a better understanding of changes that might occur in samples returned from Mars.

Keywords: gypsum, bassanite anhydrite, X-ray diffraction, Mars

INTRODUCTION

Mars is sulfur-rich, and the sulfur cycle dominates many geological processes that leave evidence in a range of sulfate phases at the surface (King and McLennan 2010). Orbital observations and exploration by landers and rovers reveal widespread calcium sulfate minerals. Gypsum ($CaSO_4 \bullet 2H_2O$) has a spectral absorption at 1940 nm that allows recognition from orbit, with the most striking example being the extensive circumpolar gypsum dune field of Olympia Undae near the north pole (Langevin et al. 2005; Fishbaugh et al. 2007). Bassanite ($CaSO_4 \bullet (\sim 0.5)H_2O$) at Mawrth Vallis was reported by Wray et al. (2010) based on Compact Reconnaissance Imaging Spectrometer for Mars (CRISM) spectral absorption at 1910 and 2480 nm. On the surface, the Mars Exploration Rover *Opportunity* used Pancam reflectance features in the 934 to 1009 nm range to identify gypsum in veins at Endeavour crater (Squyres et al. 2012). Anhydrite ($CaSO_4$), lacking water molecules, is not detectable using these spectral methods.

The CheMin X-ray diffraction (XRD) instrument on the Mars Science Laboratory (MSL) rover *Curiosity* was sent to Gale crater on Mars to examine the mineralogy of a sedimentary record of early martian environments (Grotzinger et al. 2012). Gale crater is ~5° south of the martian equator, on the dichotomy boundary between southern highlands and northern plains. Gale is ~155 km in diameter and has a ~5 km tall central mound (Aeolis Mons, informally known as Mount Sharp) of varied sediments, from lower strata with clay minerals and other hydrous phases upward through layers with sulfates of varied hydration, to higher layers that are spectrally similar to global martian dust (Milliken et al. 2010). The transition from lower strata with clay minerals to more sulfate-rich upper strata provides an opportunity to examine a stratigraphic record of local, and possibly global, environmental change on Mars.

Setting and Samples

Curiosity landed northwest of the Gale crater central mound in 2012, and is progressing to higher elevations through lower mound strata. These strata and the positions of CheMin samples are shown schematically in Figure 1 (see e.g., Fedo et al. 2017, for more detailed stratigraphy). To date, CheMin has analyzed lacustrine sediments, eolian sandstones (two with specifically sampled fracture-associated alteration), and eolian sands. All of these samples contain volcanic detritus, largely basaltic but with evidence of some evolved igneous sources, and a significant and sometimes dominant X-ray amorphous

component (Bish et al. 2013; Vaniman et al. 2014; Treiman et al. 2016; Morris et al. 2016; Rampe et al. 2017; Yen et al. 2017; Achilles et al. 2017). Sulfate is present in all, and gypsum, bassanite, and anhydrite are the most common crystalline sulfate salts.

Most samples analyzed by CheMin are targeted to emphasize matrix mineralogy rather than the common light-toned veins observed at Gale crater, although light-toned veinlets and/or nodules are unavoidable in some drill holes. At the time of writing, CheMin has analyzed seventeen samples in total. The most abundantly sampled lithology (nine samples) is lacustrine mudstone: John Klein and Cumberland from the Yellowknife Bay formation and Confidence Hills, Mojave2, Telegraph Peak, Buckskin, Marimba2, Quela, and Sebina from higher strata in the Murray formation (Vaniman et al. 2014; Rampe et al. 2017; Morris et al. 2016; Bristow et al. 2017). One sample, Oudam, is a siltstone to fine sandstone from an outcrop with large-scale cross-bedding that might be eolian. Five samples are sandstones. One sample (Windjana) within the Kimberley formation is from a cross-stratified sandstone that may represent an eolian cycle, including more alkaline-felsic detritus, within fluvio-lacustrine sediments (Treiman et al, 2016). The four other sandstones represent the Stimson formation, from dominantly basaltic sources, unconformably deposited above the Murray formation. These four samples include two of sandstone host rock (Big Sky and Okoruso) and two fracture alteration halos targeted to compare with adjacent host rock: Greenhorn, associated with Big Sky host rock, and Lubango, associated with Okoruso host rock (Yen et al. 2017). All of the above were collected as drill powders from outcrop. In addition to these 15 drill samples, two unconsolidated eolian sands were collected by scoop at Rocknest and Gobabeb (Bish et al. 2013; Achilles et al. 2017). Full CheMin mineralogical analyses of these samples, including tables of mineral abundances, are covered in the publications cited above. In this study we focus on Ca-sulfates, but describe relations with other phases where relevant to the discussion.

METHODS

X-ray Diffraction in CheMin, with specific notes on Ca-sulfate phases

CheMin collects X-ray diffraction (XRD) and X-ray fluorescence (XRF) data simultaneously using Co radiation in transmission geometry (a detailed instrument description can be found in Blake et al. 2012). Samples are obtained using either the MSL scoop (for loose sands) or the MSL drill (sedimentary rocks). Sieved sample splits of <150 μm grain size and ~ 50 mm^3 volume are delivered to CheMin analysis cells that have either Mylar or Kapton windows. Sample cells are reusable and located on a rotating sample wheel. These cells are shaken piezoelectrically during analysis to randomize grain orientations, presenting all lattice orientations to the incident Co X-rays. A CCD detector is used to determine the energy of

photons striking the CCD; fluoresced photons provide XRF data and the two-dimensional (2D) positions of diffracted Co Kα photons are used to construct the diffraction pattern. Circumferential integration of Debye diffraction rings, adjusted for arc length, produces a conventional 1D XRD pattern with 2-theta resolution of ~0.3°. Positions of diffracted photons are summed over repeated 10-sec measurements for several hours during each night of analysis. Samples are generally analyzed for four or more nights, spaced at time intervals determined by rover energy budget, allowance for operating other instruments, and other operational considerations. Plagioclase is a common phase in almost all samples, and the 1D diffraction patterns are corrected for minor variations in sample-to-detector distance using the best fit to plagioclase c and γ cell parameters (Morrison et al. in press). Abundances of crystalline phases are determined by full-pattern fitting and Rietveld analysis; the abundances of amorphous components and poorly-crystalline clay minerals are determined using the program FULLPAT (Chipera and Bish 2002).

CheMin can readily identify and quantify Ca-sulfate minerals (Figure 2). Although gypsum, bassanite, and anhydrite are common mineral names, terminology used for Ca-sulfate phases can be complex, particularly in the use of "soluble anhydrite", "γ-anhydrite", or "anhydrite III" (e.g., Bezou et al. 1995, Carbone et al. 2008, Seufert et al. 2009) for dehydrated channel structures more similar to bassanite than to common anhydrite (which lacks channel structure and hydrates less readily). In this paper, we refer to the anhydrous structure without channels simply as anhydrite, or "common anhydrite" where there may be some confusion with channel-bearing structures, such as soluble anhydrite, that are more similar to bassanite than to common anhydrite.

Crystallographic differences between bassanite and "soluble anhydrite" are subtle (Robertson and Bish 2013); at the resolution of the CheMin instrument this distinction cannot be made with confidence when Ca-sulfates are in low abundance. In this paper we use the term *bassanite* with the understanding that other channel structures are possible, but only bassanite is recognized as a naturally occurring mineral by the International Mineralogical Association. Nevertheless, there is much yet to be learned concerning channel-structure Ca-sulfates in terrestrial environments. For example, there is a recent determination of natural soluble anhydrite in the Atacama Desert, a site considered in some respects as a terrestrial analog for Mars (Wei et al. 2015).

Accounting for the sample environment inside CheMin

The CheMin operating environment can impact hydrous mineral stability and thus interpretations of *in situ* mineralogy. CheMin operates at night, at the lowest possible temperature. This is necessary because acceptable cold operating temperature for energy discrimination by the CCD detector can only be reached at night, when heat load from the rover deck is minimal. Temperature inside CheMin cycles between

nighttime lows of ~6 to 7 °C and daytime highs that average ~25 to 30 °C (Table 1 and Figure 3a). These conditions are warmer than local air temperatures (6 °C on a warm spring or summer day to -90 °C on a cold autumn or winter night). At the warmer conditions inside CheMin, sample dehydration may occur because relative humidity remains low. The volume of sample in a CheMin analysis cell (~50 mm^3) is only ~10^{-5} of the free space within the CheMin enclosure, and any water vapor lost from a sample has negligible impact on internal humidity. Moreover, the CheMin enclosure communicates with external atmosphere through a 90x90 mm HEPA filter. Water vapor inside CheMin reflects the volume mixing ratio (VMR) in the martian atmosphere, which has been estimated at nighttime using the REMS instrument on MSL and varies from ~0 to 10 ppm at solar longitude (L_s) of 50° to 90° (late autumn at Gale) to ~20 to 60 ppm at most other seasons (Martínez et al. 2017). With warmer conditions inside CheMin, the relative humidity is close to zero.

Warm conditions inside CheMin provide an opportune laboratory on Mars for mineral stability experiments. The CheMin team has studied possible mineral dehydration through exposure to post-drilling desiccating conditions, including an experiment that held a clay mineral with 13 Å basal spacing in CheMin for 150 martian solar days (referred to as sols, with a an approximate mean duration of 24 hr 39 min) to test for possible collapse to 10 Å (the clay mineral did not collapse, and is believed to be partially expanded by metal-hydroxyl groups; Bristow et al. 2015). All other clay minerals that have been analyzed in CheMin are fully collapsed; if they originally had hydrated interlayer cations, that hydration was lost before delivery and analysis. No obvious transformations were seen until CheMin analyzed the Stimson fracture sample Lubango (Figure 1), where a small amount of gypsum detected during the first night of analysis decreased below detection limits after 7 sols while bassanite increased (Table 2a). In the next sample, Oudam, there was no initial bassanite but gypsum was joined by some bassanite after 4 sols, with less gypsum and more bassanite after 8 sols, and total transformation of gypsum to bassanite after 37 sols (Table 2b and Figure 3b). Full-pattern fitting of XRD data is used to track loss of gypsum and formation of bassanite, though this transition is readily evident in the heights of diffraction peaks specific to either gypsum or bassanite (Oudam example in Figure 3c).

The external environment: Ground Temperature Sensor methods

The MSL Rover Environmental Monitoring Station (REMS) Ground Temperature Sensor (GTS) uses a mast-mounted thermopile, with sensitivity in the 8-14 μm range, to measure surface brightness temperatures. The GTS field of view is to the right of the rover, 120° from forward facing and 26° below horizontal. The area covered by the field of view is ~100 m^2, depending on rover tilt, though about half the signal comes from a small part of this area close to the rover. The GTS temperature measurements are affected by sensor performance and surface emissivity, but also by any rover shadowing and heat from

the rover's radioisotope thermoelectric generator (RTG). In this study, we use GTS data with the highest confidence possible, that is, with the Application-Specific Integrated Circuit (ASIC) power supply in its operation range, the highest recalibration quality, and with no shadows in the GTS field of view. Uncertainties in processed temperature measurements are generally <2 °C. For a more detailed description see Hamilton et al. (2014) and Martínez et al. (2017).

RESULTS

Quantitative mineral analyses of all CheMin samples are available in the NASA Planetary Data System (http://pds-geosciences.wustl.edu/msl/msl-m-chemin-4-rdr-v1/) and in condensed form in the Astrobiology Habitable Environments Database (http://odr.io/CheMin). Those repositories use best available data that represent the mineralogy of samples *in situ*. Figure 4 summarizes the *in situ* Ca-sulfate mineralogy of all CheMin samples, as reported in these data collections. For discussion later, Figure 4 also shows CheMin abundances of hematite and magnetite reported to the NASA Planetary Data System.

For gypsum-bearing samples, all of which lost gypsum and formed bassanite over several sols, the NASA Planetary Data System analyses report only data collected before gypsum began to transform to bassanite. For this paper, in order to use the CheMin instrument as a mineral stability laboratory and track the loss of gypsum and formation of bassanite, we have treated each night of analysis separately for all five gypsum-bearing samples. These analyses are listed in Tables 2a to 2e. All of these samples were analyzed within a period of 150 sols, from L_s 143° to L_s 253°, local winter to spring, when daily surface high temperatures increased from -12 °C to +10 °C and maximum air temperature increased from about -17 °C to -5 °C. Diurnal thermal cycles inside CheMin were similar for all five samples (Table 1), with maximum daytime temperatures inside CheMin ranging from 25.0 ±1.8 °C for Lubango to 30.0 ±2.5 °C for Quela. Tables 2a to 2e show that in all five of these samples gypsum began transition to bassanite inside CheMin within 3 to 4 sols, with significant losses of gypsum and formation of bassanite in 3 to 8 sols and total loss of gypsum by formation of bassanite within 8 sols for Marimba2, Quela, and Sebina. In Lubango and Oudam complete loss of gypsum with formation of bassanite took more than 7 to 8 sols. The cause of longer gypsum persistence in Lubango and Oudam is not known, but factors such as particle size have an effect (Vaniman and Chipera 2006). Variations within the 0-150 μm grain size distribution may be a factor, but it's also possible that mineral associations or the volume loaded in the sample cell may affect dehydration rate.

DISCUSSION

Ca-sulfate stratigraphy and diagenetic events

Figure 4 shows that wherever Ca-sulfates are found, anhydrite is present, despite less favorable XRD detection limits for anhydrite relative to gypsum and bassanite (Figure 2). Gypsum was only found in samples from the upper Murray formation and in the Stimson formation where the Lubango drill hole sampled a fracture-associated halo (Yen et al. 2017). Since the observation of gypsum in Oudam, it has been found in every CheMin sample higher in the Murray Formation. There is a Ca-sulfate "barren zone" in the Confidence Hills and Mojave2 drill holes, located at the base of the Murray Formation. This zone has the highest jarosite abundances yet observed at Gale crater and concretions of Mg,Ni-sulfates (Rampe et al. 2017); Mojave2 also has crystal molds that may represent late diagenetic loss of an earlier sulfate mineral (Grotzinger et al. 2015).

Bassanite plus anhydrite in the John Klein and Cumberland mudstones is attributed to small veinlets that were quantified in the Yellowknife Bay boreholes (supplement to Vaniman et al. 2014), with little or no Ca-sulfate cement in the mudstone matrix. No such veinlets were observed in the Oudam, Marimba2, Quela, and Sebina boreholes, yet the abundance of Ca-sulfates is greater than at Yellowknife Bay and represents a fine-scale component, possibly in the form of cement.

Abundant Ca-sulfate in the upper Murray formation, including gypsum, contrasts with limited Ca-sulfate and only anhydrite ± bassanite in the unconformably overlying Stimson sandstone matrix. The upper Murray also has abundant hematite (~6 wt%) and no magnetite, whereas the Stimson sandstone matrix has abundant magnetite (10 to 11 wt%) but little hematite (Figure 4). Magnetite, as well as hematite and Ca-sulfate, may be diagenetic (Yen et al. 2017). The Ca-sulfate-rich and hematite-forming oxidizing fluids present during deposition of the upper Murray formation (Bristow et al. 2017), or during a later alteration episode, did not affect the Stimson formation sandstones. This diagenesis of the upper Murray formation may predate the unconformity, or the unconformity may have been a barrier to alteration. The unconformity was studied earlier at Marias Pass, just above the Buckskin sample (Figure 1), where Ca-sulfate veins are concentrated in the Murray formation but not in the Stimson formation and there is a thin, possibly fluvial unit at the base of the Stimson with clasts of altered Murray (Edgett et al. 2016, Newsom et al. 2016). This geometry suggests that Ca-sulfate alteration predated Stimson deposition and lithification. However, there are open fractures with associated thick alteration halos, related to those in the Stimson (Greenhorn, Lubango; Yen et al. 2017), that cross the unconformity. Fracture-associated alteration halos in the Stimson have been analyzed by CheMin, but the halos in the Murray have not; nevertheless, continuity of these halos across the unconformity indicates later alteration that followed deposition and lithification of the Stimson. More than one Ca-sulfate alteration event, including fluids of various oxidation states, is implicated.

Conditions that may destabilize gypsum on Mars

As noted above, the Ca-sulfate stratigraphy in Figure 4 represents *in situ* mineralogy, acquired before gypsum destabilization inside the CheMin instrument. Gypsum takes several sols to begin transformation to bassanite inside CheMin, matching laboratory experience (Vaniman and Chipera 2006). Here we consider whether gypsum might dehydrate at the martian surface, at somewhat lower temperatures but much longer exposure.

Figure 5 shows four profiles of maximum diurnal summer temperature to 12 cm depth for mudstones at Yellowknife Bay (sol 140), in the lower Murray formation (sols 787 and 812), and at the Sebina sampling site (sol 1495). These profiles were calculated by solving the heat conduction equation using local REMS ground temperature sensor data and thermal inertia values estimated as described in Martínez et al. (2014); all analyses are for comparable seasonal conditions (mid-spring). Calculated mudstone thermal inertias (J m^{-2} K^{-1} $s^{-1/2}$) are 445 for Yellowknife Bay, 520-565 for the lower Murray, and 380 for the upper Murray at Sebina. At lower thermal inertia, the surface becomes warmer and the maximum temperature decreases more rapidly with depth. Figure 5 includes the intersection of thermal profiles with the MSL drill sampling depth of 2 to 6 cm and the daily temperature range inside CheMin for mid-spring conditions.

Based on thermal profiles, gypsum at the CheMin sampling depth of 2 to 6 cm has been stable against dehydration, or has resisted dehydration, before delivery into CheMin. Conversely, lack of gypsum in CheMin samples indicates that it was initially absent, or below detection limits. Rapin et al. (2016) analyzed ChemCam laser ablation data of H abundance and found hydration equivalent to bassanite in surface analyses of Ca-sulfate veins, at laser depths of a few micrometers. Surface bassanite could be a product of gypsum dehydration. Warm-season surface temperatures are within the range of CheMin internal temperatures where gypsum quickly (within 2 to 4 sols) transforms to bassanite. Although this transformation is fastest at the high end of the CheMin temperature range (25 to 30 °C), lower temperatures may be sufficient to dehydrate gypsum over many spring and summer seasons, where maximum early afternoon surface temperatures of ~5 to 10 °C are reached repeatedly for ~150 sols each martian year (Martínez et al. 2017).

To consider possible dehydration of gypsum in surface exposures, duration of surface exposure is a critical factor. A maximum erosion rate at Gale crater determined by Kite and Myer (2017) is 1 μm/yr (or about twice this in a martian year); at this rate a sample with thermal inertia of ~445 to 380 at 1 cm depth may repeatedly reach temperatures of ~5 to 10 °C for about an hour each day for approximately $5x10^3$ Mars years, before exposure at the surface and release to erosion. Considering only the hour of maximum temperature of each warm-season day, between L_s 180° and L_s 330° (150 sols), cumulative duration above 5 °C will be on the order of $7.5x10^5$ hours (~85 years). This consideration includes only the warm-

season thermal maxima, and the highest credible erosion rate, but this conservative duration nevertheless extends from the range of laboratory studies into the realm where geologic timescales are important. In the balance between erosion rate and surface exposure, sedimentary rocks of Gale crater will be within the warmest upper centimeter for thousands of years, with many decades of cumulative surface exposure to temperatures in the range of ~0 to 10 °C.

This exposure history could allow partial or complete transformation of gypsum to bassanite, as suggested in Rapin et al. (2016). Vaniman and Chipera (2006) found that at ~24 °C and RH <0.1%, gypsum grains from <45 μm to 425 μm began to lose water within 30 to 40 hours and reached complete desiccation to bassanite in 600 hours. In later work, using the same equipment but with gypsum in more geologically reasonable forms (satin spar, fracture selenite, and a nodular "chicken wire" evaporite), 150 hours were required for desiccation to begin, and $4x10^3$ hours (satin spar) to $4x10^4$ hours (nodular) to completely desiccate to bassanite (Figure 6). These results indicate that the time required to convert gypsum to bassanite can vary over two orders of magnitude, depending on crystal form and size.

The slower desiccation rates in "real rocks" that are shown in Figure 6 are exploratory, and more work on rates of gypsum to bassanite transition may help to constrain the settings in which gypsum may persist near the martian equator. With such knowledge it may be possible to apply Ca-sulfates as indicators of both primary aqueous processes and post-formation exposure history, but published data provide conflicting evidence for surface exposures with near-equatorial gypsum. Although our work and that of Rapin et al. (2016) indicates dehydration of gypsum to bassanite in the near surface, Squyres et al. (2012) reported gypsum, rather than bassanite, in a cm-wide vein at Endeavour crater (2.3° S latitude), about as close to the equator as Gale crater (5.4° S latitude). The identification of gypsum rather than bassanite at Endeavour is based on a small difference in Pancam reflectance at 1009 nm, but the data obtained favor gypsum over bassanite. This identification of gypsum is very similar to the MSL Mastcam indication of gypsum in some thicker veins of Yellowknife Bay at Gale crater, based on a similar reflectance spectrum slope between 937 and 1013 nm (Vaniman et al. 2014).

We also consider the possibility that further dehydration might produce common anhydrite. The gypsum to bassanite experiments of Vaniman and Chipera (2006) produced bassanite that retained a small amount of water (~0.8 wt%). Complete desiccation did not occur and anhydrite did not form. However, there are at least three field occurrences on Earth where dry desiccation of gypsum to form common anhydrite has been reported: in Death Valley, California where inactive gypsum spring deposits develop caprock of bassanite or anhydrite (Hunt et al. 1966); in disturbed evaporite sediment at Clayton Playa in Nevada (Moiola and Glover 1965); and in speleothems of shallow, dry caves at Big Bend National Park in Texas (Hill 1979). These studies attribute the transformation to dehydration without recrystallization through an

297 aqueous phase. All report summer air temperatures that reach ~35 °C or more. The Moiola and Glover
298 (1965) study has some constraints on rate and amount of transformation, for within one year they describe
299 initial wet growth of cm-scale gypsum crystals followed by dry alteration of the crystal surfaces, in which
300 a thin (~60 μm) layer of bassanite occurs between the gypsum core and an outer layer (~500 μm) of
301 common anhydrite, supporting an interpretation of progressive desiccation from the gypsum core to the
302 anhydrite rim. Laboratory experiments heating gypsum for 120 hours in air at 85 °C have produced a
303 small percentage (4%) of common anhydrite along with 95% bassanite (Seufert et al. 2009); whether
304 geologically longer exposure of gypsum at lower temperatures might also produce common anhydrite is
305 not known. Although MSL data support likelihood of some bassanite formation by desiccation from
306 gypsum, it remains unknown whether prolonged surface exposure at Gale crater might produce common
307 anhydrite as well as bassanite.

308 If dehydration to common anhydrite has occurred at Gale crater, it is most likely in dark eolian sands such
309 as Rocknest and Gobabeb. These sands have very low thermal inertia (~280 and 180 respectively) and
310 low albedo (0.21 and 0.11 respectively; Vasavada et al. 2017). The active Gobabeb dunes reach
311 temperatures ~10 °C warmer than sedimentary rocks at similar conditions (Martínez et al. 2017).
312 Moreover, the exposure age of eolian sands may be much greater than solid rock with a limited surface
313 exposure period dependent on erosion rate. Note that the only Ca-sulfate observed in Gobabeb and
314 Rocknest sands is anhydrite (Figure 4). This observation supports a hypothesis of gypsum dehydration to
315 anhydrite in dark sands at low latitude, though other explanations are possible, including either an
316 anhydrite-only source or mechanical loss of softer gypsum and bassanite in eolian processing.

317 **Pervasive anhydrite at Gale crater**

318 Perhaps common anhydrite can form by dehydration of gypsum at Gale crater, but pervasive anhydrite in
319 sedimentary rocks more likely formed by growth from solution. Given sufficient time and fluid to mediate
320 reactions, Ca-sulfate should tend toward either gypsum or anhydrite. In dilute solution, anhydrite forms at
321 somewhat elevated temperature, generally above ~40 to 60 °C (e.g., Hardie 1967; Van Driessche et al.
322 2017). However, activity of water has a significant effect and in concentrated brine anhydrite can form at
323 temperatures as low as 18 °C at water activity of 0.75, and as low ~0 °C in residual solution for a modeled
324 brine with <4% remaining fluid at Meridiani Planum (Marion et al. 2009; Marion et al. 2016). The
325 situation may also be complicated by groundwater dynamics and matrix mineralogy; in experiments with
326 $CaCl_2$ brine and a K-jarosite matrix, static batch systems precipitate only gypsum, whereas flowing
327 systems can precipitate gypsum plus anhydrite (Miller et al. 2017).

Although anhydrite formation temperature may be lowered in brines, highly soluble salts would be expected in the ultimate precipitate. There is evidence of associated Na and Cl, interpreted as halite, in the upper Murray formation (Thomas et al. 2017), though only in local concentrations. However, highly soluble Mg-sulfates are also evident as diagenetic concretions in the lower Murray formation (Rampe et al. 2017) and significant amounts of highly soluble Mg- and Fe-sulfates and perchlorates are indicated in temperatures of SO_2 gas evolution for almost all Gale crater sedimentary rocks analyzed with the MSL Sample Analysis at Mars (SAM) instrument (Sutter et al. 2017). CheMin analyses indicate that these other salts are either below detection limits (~0.1 to 0.5 wt%) or X-ray amorphous. Evident abundance in the evolved gas data suggests the latter, and Mg- or Fe-sulfates that are amorphous in CheMin may originally have been crystalline precipitates from brine.

A caveat in this discussion is that most Mg-sulfate phases (e.g., hexahydrate) dehydrate much more readily than gypsum and can dehydrate to an amorphous rather than crystalline form (Vaniman and Chipera 2006). Studies of ferric sulfates show that they too are prone to produce X-ray amorphous material on wetting and drying (Chipera et al. 2007; Morris et al. 2015). It is possible that Mg- and Fe-sulfates in MSL drill samples were crystalline *in situ*, but quickly became amorphous inside CheMin before or during the first night of analysis. More information on Gale crater salts will be acquired as *Curiosity* traverses up into more sulfate-rich strata.

IMPLICATIONS

Arrested phase transitions on Mars

In the relatively wet near-surface environments of Earth, gypsum is favored over anhydrite and bassanite (Marion et al. 2016). At Gale crater occurrence of gypsum, bassanite, and anhydrite, sometimes in close association, suggests a fluid-limited system (limited as either brief wet environments or low water/rock ratio). Bassanite, poised between gypsum dehydration and anhydrite hydration, is more common, and more likely, on water-limited Mars than on wet Earth.

Anhydrite may indicate precipitation at somewhat elevated temperature (> ~50 °C), as is often the case on Earth, but at Gale this interpretation is complicated by the various mixed-phase associations of bassanite + anhydrite, gypsum + anhydrite, and gypsum + bassanite + anhydrite. The common connection in all Ca-sulfate bearing samples is presence of anhydrite. If anhydrite formed in Gale sediments at elevated temperature, any retrograde alteration to more hydrated Ca-sulfates has been incomplete or interrupted. If anhydrite formed at low temperature by precipitation from brine, incomplete reaction with solution or fluid isolation has preserved gypsum and bassanite. In either case, as with persistence of bassanite in

association with anhydrite and gypsum, the evidence points to low water/rock ratios and low temperature favoring incomplete reaction.

Complexity of "ground truth" at Mount Sharp

Observations of Mars from orbit have provided extensive maps of mineral distributions, but those maps are limited by scale of resolution, dust cover, and other factors that challenge remote mineral determinations. In addition, the maps obtained are limited to those minerals that provide detectable signatures from a distance. Thus mapping of phases such as clay minerals, hydrated salts, and hematite, as examples, are generally represented by the phases that dominate in the range of the detector, producing a generally monomineralic or simplified mineralogic view. Moreover, important phases that are invisible to remote detection, such as anhydrite, will be missed. Landers with close-up and contact instruments provide a chance to obtain "ground truth" for comparison with orbital maps and can fill in such gaps.

The CheMin results at Gale crater can be compared with detailed orbital mapping prior to and during the Mars Science Laboratory mission. The results for Ca-sulfates have been informative, but also present their own complexity in interpretation. Gypsum destabilization within CheMin illustrates the need to assess possible perturbation of a sample as it is collected and processed, but analyses of such transformations can also provide *in situ* constraints on mineral stability that would not otherwise be possible. At Gale crater, several of the minerals observed with orbital mapping (e.g., Milliken et al. 2010, Lane and Christensen 2013, Fraeman et al. 2016) have been verified on the ground, beginning with hematite in the Murray Formation. However, there has been no confident orbital detection of Ca-sulfates at Gale crater. The results from Mars Science Laboratory to date show that Ca-sulfates are almost pervasive throughout the lower strata of Mount Sharp. Other salts, notably kieserite and polyhydrated Mg-sulfates, are indicated at Mount Sharp from orbit (Milliken et al. 2010), dominantly in strata above the present location of the rover, that may represent a marked change of environment. Hydrated sulfates other than Ca-sulfates are present as part of the X-ray amorphous material in CheMin samples, but it will require analyses of sulfate-rich strata higher up-section to confirm the crystalline versus amorphous salt components and their relations with the Ca-sulfates.

Mineral stability can impact mineral analysis on and sample return from Mars

It is evident from CheMin analyses of gypsum that the act of sampling and analysis can produce mineral transformations through dehydration. The transformation of gypsum to bassanite is clearly observed in CheMin XRD analyses. To relate observations within CheMin to mineralogy *in situ*, adjunct data are needed from thermal sensors within CheMin as well as data from the REMS Ground Temperature Sensor. ChemCam analyses of surface hydrogen abundances in veins and SAM evolved gas analyses support

these interpretations. Multiple instrumentation is of great importance for sample analyses on Mars. *In-situ* analyses and documentation will be even more important when returning martian samples to Earth. Simple dehydration is not the only process that must be considered; reactions between hydrous phases may also be driven by changes in temperature and relative humidity (e.g., cation exchange reactions between clay minerals and Mg-sulfates in the absence of free-liquid H_2O, accompanied by formation of gypsum or bassanite where thin skins of water may have formed; Wilson and Bish 2011). Broader concerns such as this, and the limitations in ability to fully prevent any such transformations, are a concern recognized in sample return strategies for Mars. For return of samples to Earth, encapsulation and monitoring of thermal history may not prevent mineral transformations but will provide a basis for unravelling such processes (MEPAG 2008). Bringing mutable phases out of their "comfort zone" *in situ* provides new understanding of what transformations are likely. The CheMin experience with gypsum dehydration on Mars provides another empirical data point on the long path toward sample return from Mars to Earth.

ACKNOWLEGMENTS

This paper was improved with helpful reviews by Ron Peterson and Melissa Lane. Support from the NASA Mars Science Laboratory Mission for CheMin development and operation is gratefully acknowledged. Sulfate stability work by dtv and sjc was supported through Los Alamos National Laboratory Directed Research and Development funding, and NASA grant NNH10A083I.

REFERENCES CITED

Achilles, C.N., Downs, R.T., Ming, D.W., Rampe, E.B., Morris, R.V., Treiman, A.H., Morrison, S.M., Blake, D.F., Vaniman, D.T., Ewing, R.C., and others. (2017) Ground truth mineralogy vs. orbital observations at the Bagnold dune field. Lunar and Planetary Science XLVIII, abstract 2889.

Bezou, C., Nonat, A., Mutin J.-C., Nørlund Christensen, A., and Lehmann, M.S. (1995) Investigation of the crystal structure of γ-$CaSO_4$, $CaSO_4$•$0.5H_2O$, and $CaSO_4$•$0.6H_2O$ by powder diffraction methods. Journal of Solid State Chemistry, 117, 165-176.

Bish, D.L., Blake, D.F., Vaniman, D.T., Chipera, S.J., Morris, R.V., Ming, D.W., Treiman, A.H., Sarrazin, P., Morrison, S.M., Downs, R.T., and others. (2013) X-ray diffraction results from Mars Science Laboratory: Mineralogy of Rocknest at Gale crater: Science, 341, doi:10.1126/Science.1238932.

Blake, D., Vaniman, D., Achilles, C., Anderson, R., Bish, D., Bristow, T., Chen, C., Chipera, S., Crisp, J., Des Marais, D., and others. (2012) Characterization and calibration of the CheMin mineralogical instrument on Mars Science Laboratory: Space Science Reviews, doi:10.1007/s11214-012-9905-1.

Boeyens, J.C.A., and Ichharam, V.V.H. (2002) Redetermination of the crystal structure of calcium sulphate dihydrate, $CaSO_4$•$2H_2O$. Zeitschrift für Kristallographie. New crystal structures, 217, 9-10.

Bristow, T.F., Bish, D.L., Vaniman, D.T., Morris, R.V., Blake, D.F., Grotzinger, J.P., Rampe, E.B., Crisp, J.A., Achilles, C.N., Ming, D.W., and others. (2015) The origin and implications of clay minerals from

Yellowknife Bay, Gale crater, Mars. American Mineralogist, 100, 824-826, doi:10.2138/am-2015-5077.

Bristow, T.F., Blake, D.F., Vaniman, D.T., Chipera, S.J., Rampe, E.B., Grotzinger, J.P., McAdam, A.C., Ming, D.W., Morrison, S.M., Yen, A.S., and others. (2017) Surveying clay mineral diversity in the Murray Formation, Gale crater, Mars. Lunar and Planetary Science XLVIII, abstract 2462.

Carbone, M., Ballirano, P., and Caminiti, R. (2008) Kinetics of gypsum dehydration at reduced pressure: an energy dispersive X-ray diffraction study. European Journal of Mineralogy, 20, 621-627.

Chipera, S.J., and Bish, D.L. (2002) FULLPAT: A full-pattern quantitative analysis program for X-ray powder diffraction using measured and calculated patterns. Journal of Applied Crystallography, 35, 744-749.

Chipera, S.J., Vaniman, D.T., and Bish, D.L. (2007) The effect of temperature and water on ferric-sulfates. Lunar and Planetary Science XXXVIII, abstract 1409.

Edgett, K.S., Yingst, R.A., Edgar, L.A., Gasda, P.A., Banham, S.G., Grotzinger, J.P., Newsom, H.E., Bridges, N.T., Watkins, J.A., Herkenhoff, K.E., and others. (2016) Recent observations by Curiosity's Mars Hand Lens Imager (MAHLI) of rock strata and eolian sediment on the lower north slope of Aeolis Mons, Gale crater, Mars. Lunar and Planetary Science XLVII, abstract 1382.

Fedo, C., Grotzinger, J., Gupta, S., Stein, N.T., Watkins, J., Banham, S., Edgett, K.S., Minitti, M., Schieber, J., Siebach, K., and others. (2017) Facies analysis and basin architecture of the upper part of the Murray Formation, Gale crater, Mars. Lunar and Planetary Science XLVIII, abstract 1689.

Fishbaugh, K.E., Poulet, F., Chevrier, V., Langevin, Y., and Bibring, J.-P. (2007) On the origin of gypsum in the Mars north polar region. Journal of Geophysical Research, 112, E07002, doi:10.1029/2006JE002862.

Fraeman, A.A., Ehlmann, B.L., Arvidson, R.E., Edwards, C.S., Grotzinger, J.P., Milliken, R.E., Quinn, D.P., and Rice, M.S. (2016) The stratigraphy and evolution of lower Mount Sharp from spectral, morphological, and thermophysical orbital data sets. Journal of Geophysical Research, 121, 1713-1736, doi:10.1002/2016JE005095.

Grotzinger, J.P., Crisp, J., Vasavada, A.R., Anderson, R.C., Baker, C.J., Barry, R., Blake, D.F., Conrad, P., Edgett, K.S., Ferdowski, B., and others. (2012) Mars Science Laboratory mission and science investigation. Space Science Reviews, 170, 5-56, doi:10.1007/s11214-012-9892-2.

Grotzinger, J.P., Gupta, S., Malin, M.C., Rubin, D.M., Schieber, J., Siebach, K., Sumner, D.Y., Stack, K.M., Vasavada, A.R., Arvidson, R.E., and others. (2015) Deposition, exhumation, and paleoclimate of an ancient lake deposit, Gale crater, Mars. Science, 350, doi: 10.1126/science.aac7575.

Hamilton, V.E., Vasavada, A.R., Sebastián, E., de la Torre Juárez, M., Ramos, M., Armiens, C., Arvidson, R.E., Carrasco, I., Christensen, P.R., De Pablo, M.A., and others. (2014) Observations and preliminary science results from the first 100 sols of MSL Rover Environmental Monitoring Station ground temperature sensor measurements at Gale crater. Journal of Geophysical Research, Planets, 119, 745-770, doi:10.1002/2013JE004520.

Hardie, L.A. (1967) The gypsum-anhydrite equilibrium at one atmosphere pressure. American Mineralogist, 52, 171-200.

Hawthorne, F.C., and Ferguson, R.B. (1975) Anhydrous sulphates. II. Refinement of the crystal structure of anhydrite. Canadian Mineralogist, 13, 289-292.

Hill, C.A. (1979) Recent anhydrite and bassanite from caves in Big Bend National Park, Texas. National Speleological Society Bulletin, 42, 126-127.

Hunt, C.B., Robinson, T.W., Bowles, W.A., and Washburn, A.L. (1966) Hydrologic basin Death Valley California. U. S. Geological Survey Professional Paper 494-B, 138 p.

King, P.L., and McLennan, S.M. (2010) Sulfur on Mars. Elements, 6, 107-112, doi:10.2113/gselements.6.2.107.

Kite, E.S., and Myer, D.P. (2017) Mars sedimentary rock erosion rates constrained using crater counts, with applications to organic-matter preservation and to the global dust cycle. Icarus, 286, 212-222, doi.org/10.1016/j.icarus.2016.10.010.

Lane, M.D., and Christensen, P.R. (2013) Determining olivine compositions of basaltic dunes in Gale crater, Mars from orbit: Awaiting ground truth from Curiosity. Geophysical Research Letters, 40, 3517-3521, doi:10.1002/grl.50621

Langevin, Y., Poulet, F., Bibring, J.-P., and Gondet, B. (2005) Sulfates in the north polar region of Mars detected by OMEGA/Mars Express. Science, 307, 1584-1586, doi:10.1126/science.1109091.

Marion, G.M., Catling, D.C., and Kargel, J.S. (2009) Br/Cl partitioning in chloride minerals in the Burns formation on Mars. Icarus, 200, 436-445, doi:10.1016/j.icarus.2008.12.004.

Marion, G.M., Catling, D.C., Kargel, J.S., and Crowley, J.K. (2016) Modeling calcium sulfate chemistries with applications to Mars. Icarus, 278, 31-37, doi:10.1016/j.icarus.2016.05.016.

Martínez, G.M., Rennó, N., Fischer, E., Borlina, C.S., Hallet, B., de la Torre Juárez, M., Vasavada, A.R., Ramos, M., Hamilton, V., Gomez-Elvira, J., and Haberle, R.M. (2014) Surface energy budget and thermal inertia at Gale crater: Calculations from ground-based measurements. Journal of Geophysical Research: Planets, 119, 1822-1838, doi:10.1002/2014JE004618.

Martínez, G.M., Newman, C.N., De Vicente-Retortillo, A., Fischer, E., Renno, N.O., Richardson, M.I., Farién, A.G., Genzer, M., Guzewich, S.D., Haberle, R.M., and others. (2017) The modern near-surface martian climate: A review of in-situ meteorological data from Viking to Curiosity. Space Science Reviews, doi:10.1007/s11214-017-0360.

MEPAG Mars Exploration Program Analysis Group (2008) Science priorities for Mars sample return. Astrobiology, 8, doi:1089/ast.2008.0759.

Miller, K.M., Phillips-Lander, C.M., Bishop, J.L., Elwood Madden, A.S., and Elwood Madden, M.E. (2017) Anhydrite nucleation and growth at low temperatures: Effects of flow rate, activity of water, and mineral substrates. Lunar and Planetary Science XLVII, abstract 2133.

Milliken, R.E., Grotzinger, J.P., and Thomson, B.J. (2010) Paleoclimate of Mars as captured by the stratigraphic record in Gale crater. Geophysical Research Letters, 37, L04201, doi:10.1029/2009GL041870.

Moiola, R.J., and Glover, E.D. (1965) Recent anhydrite from Clayton playa, Nevada. American Mineralogist, 50, 2063-2069.

Morris, R.V., Rampe, E.B., Graff, T.G., Archer, P.D., Le, L., Ming, D.W., and Sutter, B. (2015) Transmission X-ray diffraction (XRD) patterns relevant to the MSL CheMin amorphous component: Sulfates and silicates. Lunar and Planetary Science XLVI, abstract 2434.

Morris, R.V., Vaniman, D.T., Blake, D.F., Gellert, R., Chipera, S.J., Rampe, E.B. Ming, D.W., Morrison, S.M., Downs, R.T., Treiman, A.H., and others. (2016) Silicic volcanism on Mars evidenced by tridymite in high-SiO_2 sedimentary rock at Gale crater. Proceedings of the National Academy of Science, doi:10.1073/pnas.1607098113.

Morrison, S.M., Downs, R.T., Blake, D.F., Vaniman, D.T., Ming, D.W., Hazen, R.M., Treiman, A.H., Achilles, C.N., Yen, A.S., Morris, R.V., and others. (in press) Crystal chemistry of martian minerals from Bradbury Landing through Naukluft Plateau, Gale crater, Mars. American Mineralogist.

Newsom, H.E., Belgacem, I., Jackson, R., Ha, B., Vaci, Z., Wiens, R.C., Frydenvang, J., Gasda, P., Lanza, N., Clegg, S., and others. (2016) The materials at an unconformity between the Murray and Stimson formations at Marias Pass, Gale crater, Mars. Lunar and Planetary Science XLVII, abstract 2397.

Rampe, E.B., Ming, D.W., Blake, D.F., Bristow, T.F., Chipera, S.J., Grotzinger, J.P., Morris, R.V., Morrison, S.M., Vaniman, D.T., Yen, A.S., and others. (2017) Mineralogy of an ancient lacustrine mudstone succession from the Murray formation, Gale crater, Mars. Earth and Planetary Science Letters, 471, 172-185, doi.org/10.1016/j.epsl.2017.04.021.

Rapin, W., Meslin, P.-Y., Maurice, S., Vaniman, D., Nachon, M., Mangold, N., Schröder, S., Gasnault, O., Forni, O., Wiens, R.C., and others. (2016) Hydration state of calcium sulfates in Gale crater, Mars: Identification of bassanite veins. Earth and Planetary Science Letters, 452, 197-205, doi:10.1016/j.epsl.2016.07.045.

Robertson, K., and Bish, D. (2013) Constraints on the distribution of $CaSO_4 \cdot nH_2O$ phases on Mars and implications for their contribution to the hydrological cycle. Icarus, 223, 407-417, doi:/10.1016/j.icarus.2012.10.028.

Seufert, S., Hesse, C., Goetz-Neunhoeffer, F., and Neubauer, J. (2009) Discrimination of bassanite and anhydrite III dehydrated from gypsum at different temperatures. Zeitschrift für Kristallographie Supplements, v. 30, 447-452, doi:10.1524/zksu.2009.0066.

Squyres, S.W., Arvidson, R.E., Bell, J.F. III, Calef, F. III, Clark, B.C., Cohen, B.A., Crumpler, L.A., de Souza, P.A. Jr., Farrand, W.H., Gellert, R., and others. (2012) Ancient impact and aqueous processes at Endeavour crater, Mars. Science, 336, 570-575, doi:10.1126/science.1220476.

Sutter, B., McAdam, A.C., Mahaffy, P.R., Ming, D.W., Edgett, K.S., Rampe, E.B., Eigenbrode, J.L., Franz, H.B., Freissinet, C., Grotzinger, J.P., and others. (2017) Evolved gas analyses of sedimentary rocks and eolian sediment in Gale crater, Mars: Results of the Curiosity rover's Sample Analysis at Mars (SAM) Instrument from Yellowknife Bay to the Namib Dune. Journal of Geophysical Research-Planets, doi:10.1002/2016JE005225.

Thomas, N.H., Ehlmann, B.L., Anderson, D.E., Rapin, W., Schröder, S., Forni, O., Clegg, S.M., Wiens, R.C., Gasnault, O., and Maurice, S. (2017) ChemCam survey of volatile elements in the Murray Formation, Gale crater, Mars. Lunar and Planetary Science XLVIII, abstract 2756.

Treiman A.H., Bish, D.L., Vaniman, D.T., Chipera, S.J., Blake, D.F., Ming, D.W., Morris, R.V., Bristow, T.F., Morrison, S.M., Baker, M.B., and others. (2016) Mineralogy, provenance, and diagenesis of a potassic basaltic sandstone on Mars: CheMin X-ray diffraction of the Windjana sample (Kimberley area, Gale crater). Journal of Geophysical Research, Planets, 121, 75–106, doi:10.1002/2015JE004932.

Van Driessche, A.E.S., Stawski, T.M., Benning, L.G., and Kellermeier, M. (2017) Calcium sulfate precipitation throughout its phase diagram. Ch. 12 in New Perspectives on Mineral Nucleation and Growth, Springer, doi:10.1007/978-3-319-45669-0_12.

Vaniman, D.T., and Chipera, S.J. (2006) Transformations of Mg- and Ca-sulfate hydrates in Mars regolith. American Mineralogist, 91, 1628-1642, doi:10.2138/am.2006.2092.

Vaniman, D.T., Bish, D.L., Ming, D.W., Bristow, T.F., Morris, R.V., Blake, T.F., Chipera, S.J., Morrison, S.M., Treiman, A.H., Rampe, E.B., and others. (2014) Mineralogy of a mudstone at Gale crater, Yellowknife Bay, Mars. Science, 343, doi:10.1126/science.1243480.

Vasavada, A.R., Piqueux, S., Lewis, K.W., Lemmon, M.T. and Smith, M.D. (2017) Thermophysical properties along Curiosity's traverse in Gale crater, Mars, derived from the REMS ground temperature sensor. Icarus, 284, 372-386, doi:10.1016/j.icarus.2016.11.035.

Wei, J., Wang, A., Lambert, J.L., Wettergreen, D., Cabrol, N., Warren-Rhodes, K., and Zacny, K. (2015) Autonomous soil analysis by the Mars Microbeam Raman Spectrometer (MMRS) on-board a rover in the Atacama Desert: A terrestrial test for planetary exploration. Journal of Raman Spectroscopy, doi:10.1002/jrs.4656.

Wilson, S.A., and Bish, D.L. (2011) Formation of gypsum and bassanite by cation exchange reactions in the absence of free-liquid H_2O: Implications for Mars. Journal of Geophysical Research, 116, E09010, doi:10.1029/2011JE003853.

Wray, J.J., Squyres, S.W., Roach, L.H., Bishop, J.L., Mustard, J.F., and Noe Dobrea, E.Z. (2010) Identification of the Ca-sulfate bassanite in Mawrth Vallis, Mars. Icarus, 209, 416-421, doi:10.1016/j.icarus.2010.06.001.

Yen, A.S., Ming, D.W., Vaniman, D.T., Gellert, R., Blake, D.F., Morris, R.V., Morrison, S.M., Bristow, T.F., Chipera, S.J., Edgett, K.S., and others. (2017) Multiple stages of aqueous alteration along fractures in mudstone and sandstone strata in Gale crater, Mars. Earth and Planetary Science Letters, 47, 186-198, doi:org/10.1016/j.epsl.2017.04.033.

FIGURE CAPTIONS

Figure 1: CheMin sample types and sample locations (schematic); Stimson formation is unconformable above Murray formation. Fractures that host Greenhorn (altered Big Sky) and Lubango (altered Okoruso) cross the unconformity. Rocknest sand is from an inactive eolian deposit; Gobabeb sand is from an active eolian dune.

Figure 2: Library 1D diffraction patterns for gypsum (Boeyens and Ichharam 2002), bassanite (Bezou et al. 1995), soluble anhydrite (γ-anhydrite; Bezou et al. 1995), and common anhydrite (Hawthorne and Ferguson 1975) at CheMin 2-theta resolution (~0.3°). CheMin detection limits for gypsum and bassanite are ~0.1 wt%; the detection limit for common Amma anhydrite is less favorable (~0.2 wt%) largely because this structure lacks distinctive reflections in the area with few peak overlaps below 20°. Bassanite and C222 soluble anhydrite have very similar structures and are not readily distinguished with CheMin (differences in intensity at 34 to 38 degrees are generally masked by more abundant plagioclase and pyroxene); for this reason these phases are not distinguished in this study and only the IMA recognized mineral name bassanite is used.

Figure 3: Analysis of temperature cycles within CheMin with example of Oudam gypsum to bassanite transition; (a) diurnal temperature cycle from the 1st to 37th sol of Oudam residence inside CheMin; (b) abundance of anhydrite, bassanite and gypsum in Oudam for each of the four nights of CheMin analysis; (c) distinctive XRD peaks for gypsum and bassanite, showing progressive loss of gypsum and formation of bassanite in Oudam. The peak at 16 degrees includes diffraction from plagioclase and pyroxene.

Figure 4: Cumulative abundances of gypsum, bassanite, anhydrite, and cumulative magnetite and hematite, in all CheMin samples. Note unconformity between Murray and Stimson formations. Mineral abundances are in weight percent as a proportion of the total sample including X-ray amorphous and clay mineral components; for gypsum-bearing samples these analyses represent only those data collected before gypsum began to dehydrate to bassanite. Note full oxidation to hematite and absence of magnetite in the upper Murray formation (Oudam to Sebina), contrasted with relatively little oxidation of magnetite in the Stimson formation host rock (Big Sky, Okoruso) or in the fracture halos within the Stimson (Greenhorn, Lubango) that cross the Stimson/Murray unconformity.

Figure 5: Maximum early-afternoon warm-season diurnal temperature profiles from surface to 12 cm depth, modeled from REMS Ground Temperature Sensor data for mudstone outcrops at four different sols, with calculated thermal inertias (I). Drill samples for CheMin come from a depth of 2 to 6 cm; diurnal temperature inside CheMin ranges from ~6 to 30 °C.

Figure 6: Dehydration rates for transformation of gypsum to bassanite at 24 °C and ~0.7 Pa P_{H2O}. Rates for powdered (<45 μm) to granular (180-425 μm) samples are after Vaniman and Chipera (2006; intermediate curves are for 45-75 μm and 75-180 μm). Longer dehydration rates are for solid cm-scale (2 to 3 g) samples of satin spar (Wildhorse Mesa, Utah, crosses), single selenite crystals (Bingham, New Mexico, diamonds), and nodular evaporite (Todilto formation, New Mexico, triangles). The larger solid samples were run as duplicates and variation in duplicate rates represents variation between sample splits.

This is a preprint, the final version is subject to change, of the American Mineralogist (MSA)
Cite as Authors (Year) Title. American Mineralogist, in press.
DOI: https://doi.org/10.2138/am-2018-6346

618 **TABLES**

619 Table 1: Maximum, minimum, and average temperatures inside CheMin for analyses of gypsum-bearing
620 samples, based on CheMin interior PRT (platinum resistance thermocouple) number 2615.

	Lubango	Oudam	Marimba2	Quela	Sebina
Sol range	1323-1350	1361-1399	1425-1437	1470-1481	1496-1507
L_s range	143°-157°	163°-184°	200°-208°	229°-236°	246°-253°
Maximum °C	27.9	31.8	35.3	33.7	30.8
Average daily max °C	25.0 ±1.8	28.2 ±1.8	31.2 ±2.8	30.0 ±2.5	28.5 ±1.8
Minimum °C	6.3	6.3	6.6	6.6	6.9
Average °C*	12.8	15.3	15.5	14.7	14.5

621 "Sol" refers to sequential martian solar days of the MSL mission; L_s is solar longitude (at Gale, 0-90 =
622 autumn, 90-180 = winter; 180-270 = spring; 270-360 = summer).
623 *The average is time-adjusted to account for variable times between thermocouple readings.
624
625

Table 2a: Mineral wt% for each of four nights of analysis of the Stimson fracture sample Lubango

mineral	1st sol	4th sol	7th sol	27th sol
Andesine	12.8(5)	12.9(5)	10.5(4)	11.9(5)
Hematite	0.7(1)	0.9(2)	0.8(1)	0.9(1)
Magnetite	2.8(3)	3.1(3)	2.8(3)	2.3(2)
Anhydrite	2.8(2)	3.1(3)	4.2(4)	2.9(3)
Bassanite	2.0(2)	2.5(2)	3.1(3)	3.0(2)
Gypsum	0.9(1)	0.6(1)	0.4(1)	0.0
Pyroxene	3.8(4)	2.8(3)	4.2(4)	4.8(5)
Quartz	1.3(2)	1.0(2)	1.0(2)	1.1(2)
Amorphous	73(18)	73(18)	73(18)	73(18)

1σ analytical errors are in parentheses.

Table 2b: Mineral wt% for each of four nights of analysis of the Murray siltstone sample Oudam

mineral	1st sol	4th sol	8th sol	37th sol
Andesine	31.5(7)	31.6(7)	32.3(6)	32.1(7)
Hematite	16.3(11)	15.8(10)	15.7(10)	15.7(11)
Anhydrite	3.2(3)	3.7(4)	3.4(3)	3.4(3)
Bassanite	0.0	0.1(1)	1.8(2)	3.9(3)
Gypsum	3.3(3)	3.4(3)	1.8(2)	0.0
Pyroxene	5.7(6)	5.3(5)	5.0(5)	5.0(5)
Quartz	1.2(2)	1.1(2)	1.3(2)	1.0(2)
Clay minerals	3.3(12)	3.3(12)	3.3(12)	3.3(12)
Amorphous	35.5(90)	35.5(90)	35.5(90)	35.5(90)

1σ analytical errors are in parentheses.

Table 2c: Mineral wt% for each of four nights of analysis of the Murray mudstone sample Marimba2

mineral	1st sol	3rd sol	8th sol	11th sol
Andesine	17.3(4)	18.0(4)	17.4(3)	17.8(4)
Sanidine	2.8(8)	2.9(8)	2.7(8)	2.3(7)
Hematite	6.7(6)	6.5(6)	7.1(7)	6.7(7)
Anhydrite	3.4(3)	3.6(3)	1.5(2)[a]	1.8(2)[a]
Bassanite	0.6(2)	0.9(2)	1.8(2)	1.9(2)
Gypsum	2.2(2)	0.6(1)	0.0	0.0
Pyroxene	1.3(2)	1.7(2)	3.1(3)[a]	3.5(4)[a]
Forsterite	1.7(4)	1.6(4)	2.2(5)	1.7(4)
Jarosite	0.5(2)	0.7(2)	0.6(2)	0.6(2)
Quartz	0.3(1)	0.5(1)	0.8(2)	0.7(2)
Clay minerals	23(9)	23(9)	23(9)	23(9)
Amorphous	40(11)	40(11)	40(11)	40(11)

1σ analytical errors are in parentheses.

[a]Loss of anhydrite and increase of pyroxene in the last two nights of analysis may be caused by either grain segregation or grain ejection from the sample cell.

Table 2d: Mineral wt% for each of four nights of analysis of the Murray mudstone sample Quela

mineral	1st sol	5th sol	7th sol	10th sol
Andesine	14.3(4)	13.7(4)	13.7(3)	13.6(3)
Sanidine	1.7(5)	2.4(6)	2.0(5)	1.8(5)
Hematite	6.6(7)	7.0(7)	6.6(7)	6.5(6)
Anhydrite	3.3(3)	3.6(3)	3.6(3)	3.5(3)
Bassanite	1.5(2)	1.3(2)	1.6(2)	1.6(2)
Gypsum	0.4(1)	0.1(1)	0.0	0.0
Pyroxene	2.4(3)	2.2(2)	2.6(3)	2.8(3)
Forsterite	1.1(3)	0.9(2)	1.2(3)	1.2(3)
Jarosite	0.4(2)	0.5(2)	0.4(2)	0.6(2)
Quartz	0.4(1)	0.6(2)	0.4(1)	0.6(2)
Clay minerals	16.3(40)	16.3(40)	16.3(40)	16.3(40)
Amorphous	51.5(125)	51.5(125)	51.5(125)	51.5(125)

1σ analytical errors are in parentheses.

Table 2e: Mineral wt% for each of four nights of analysis of the Murray mudstone sample Sebina

mineral	1st sol	5th sol	7th sol	11th sol
Andesine	11.8(3)	12.0(3)	12.6(3)	12.7(4)
Sanidine	1.6(5)	1.7(5)	1.2(4)	0.9(4)
Hematite	6.2(6)	6.6(7)	6.5(7)	6.5(6)
Anhydrite	4.8(4)	5.1(5)	5.2(5)	5.1(5)
Bassanite	0.6(2)	0.8(2)	0.9(2)	1.1(2)
Gypsum	1.0(1)	0.5(1)	0.0	0.0
Pyroxene	2.4(3)	2.1(2)	1.8(2)	2.1(2)
Forsterite	0.9(2)	0.7(2)	0.9(2)	1.1(3)
Jarosite	0.8(2)	0.8(2)	0.8(2)	0.8(2)
Quartz	0.4(1)	0.2(1)	0.4(1)	0.4(1)
Clay minerals	18.5(45)	18.5(45)	18.5(45)	18.5(45)
Amorphous	51(13)	51(13)	51(13)	51(13)

1σ analytical errors are in parentheses.

This is a preprint, the final version is subject to change, of the American Mineralogist (MSA)
Cite as Authors (Year) Title. American Mineralogist, in press.
DOI: https://doi.org/10.2138/am-2018-6346

Figure 1

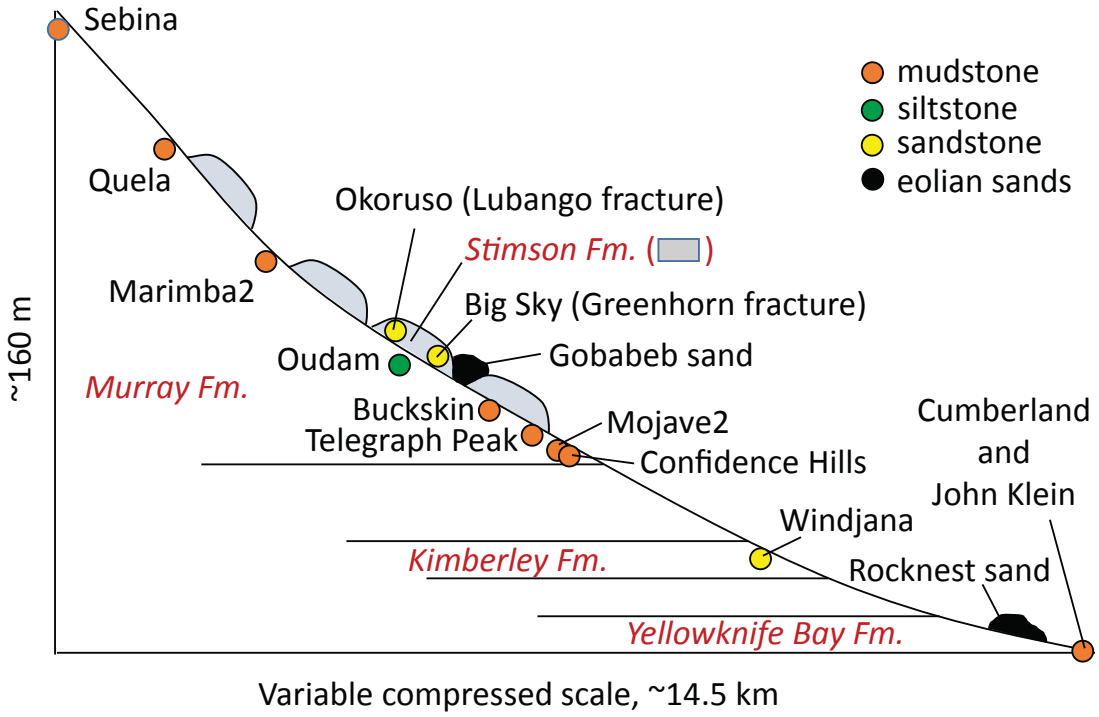

This is a preprint, the final version is subject to change, of the American Mineralogist (MSA)
Cite as Authors (Year) Title. American Mineralogist, in press.
DOI: https://doi.org/10.2138/am-2018-6346

Figure 2

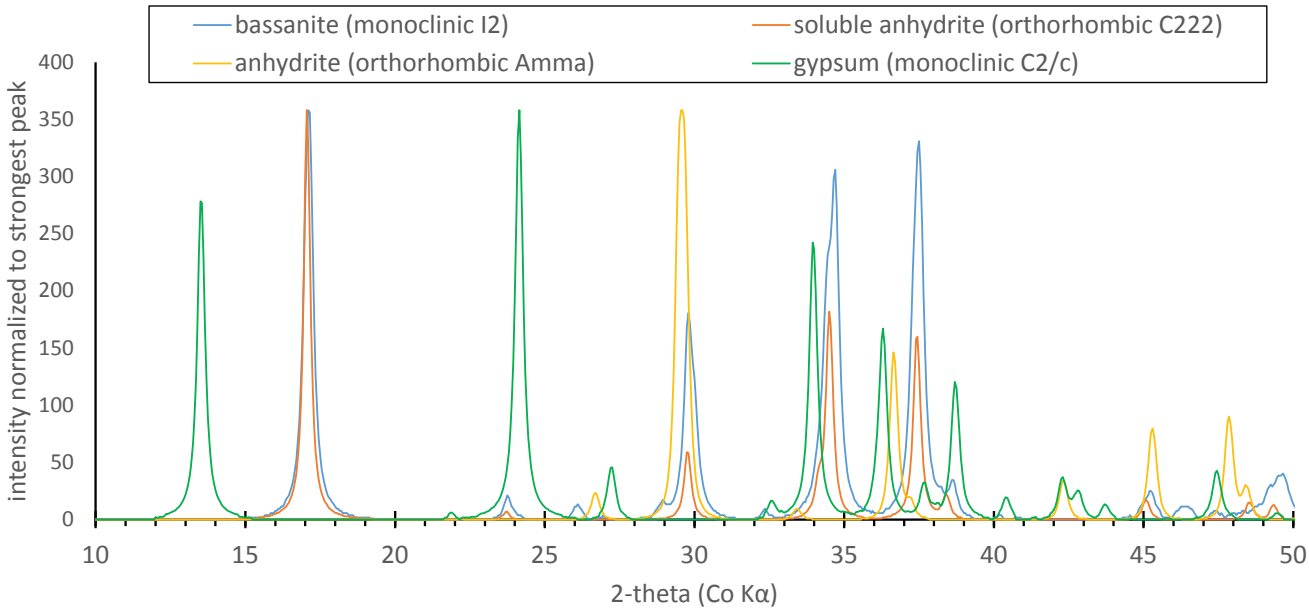

This is a preprint, the final version is subject to change, of the American Mineralogist (MSA)
Cite as Authors (Year) Title. American Mineralogist, in press.
DOI: https://doi.org/10.2138/am-2018-6346

Figure 3

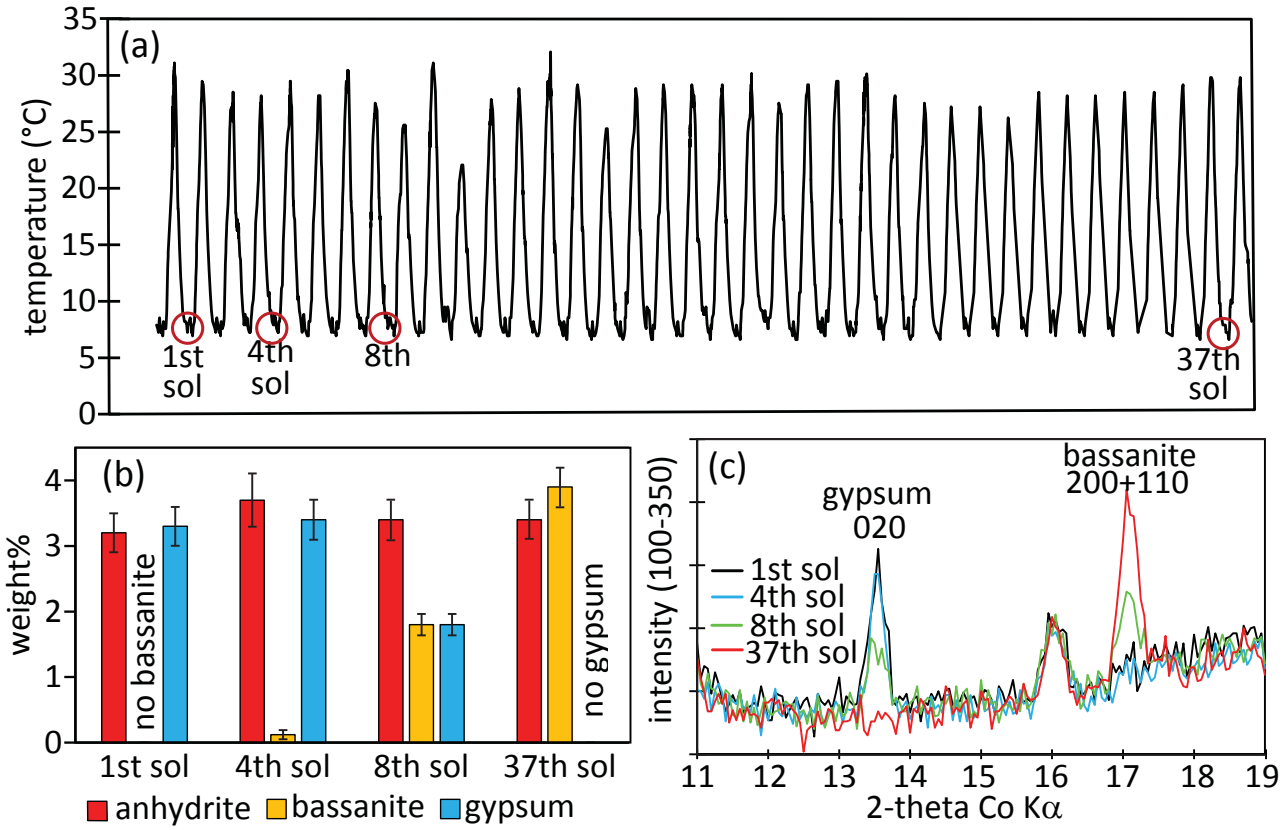

This is a preprint, the final version is subject to change, of the American Mineralogist (MSA)
Cite as Authors (Year) Title. American Mineralogist, in press.
DOI: https://doi.org/10.2138/am-2018-6346

Figure 4

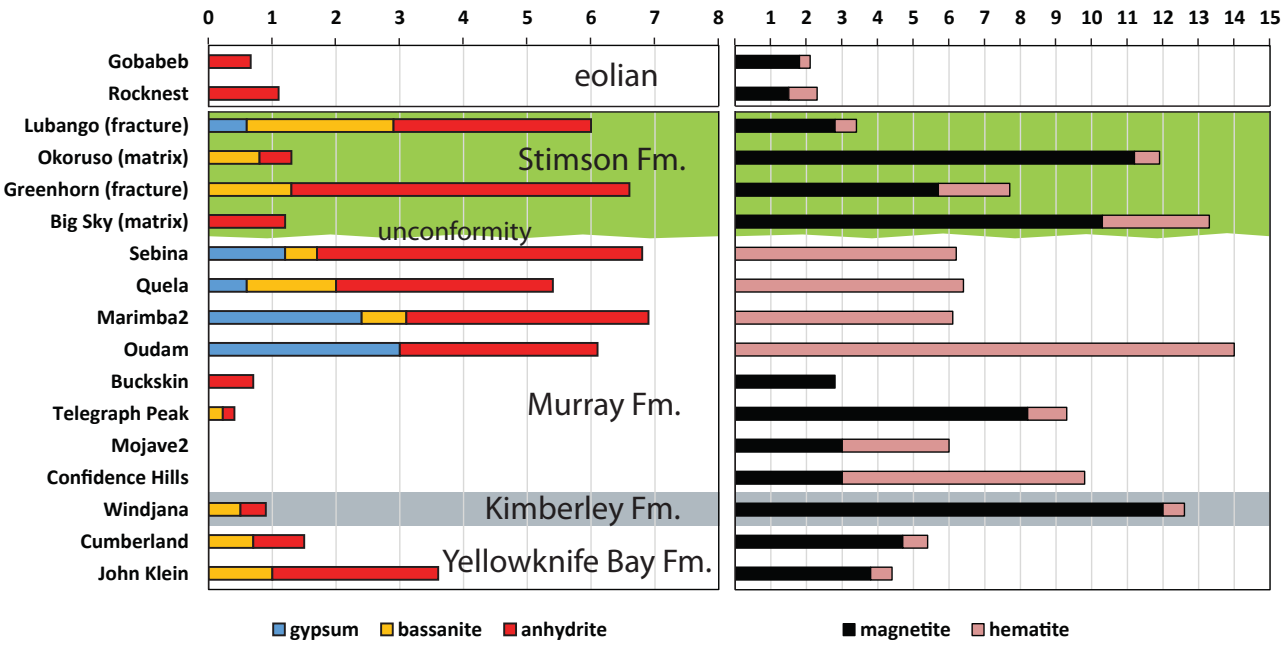

This is a preprint, the final version is subject to change, of the American Mineralogist (MSA)
Cite as Authors (Year) Title. American Mineralogist, in press.
DOI: https://doi.org/10.2138/am-2018-6346

Figure 5

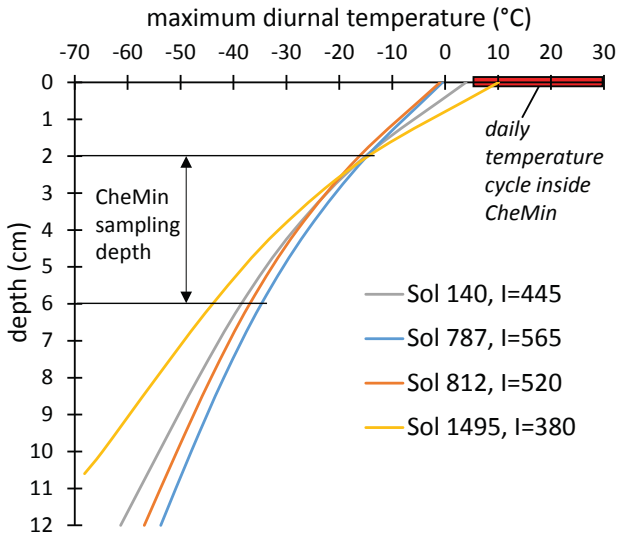

This is a preprint, the final version is subject to change, of the American Mineralogist (MSA)
Cite as Authors (Year) Title. American Mineralogist, in press.
DOI: https://doi.org/10.2138/am-2018-6346

Figure 6